

Diffraction characterization of rough films formed under stable and unstable growth conditions

J. Wollschläger, E. Z. Luo, and M. Henzler

Institut für Festkörperphysik, Universität Hannover, Appelstrasse 2, D-30167 Hannover, Germany

(Received 28 July 1997)

Characterizing the roughness of epitaxial films by diffraction techniques with respect to the step density and the rms roughness is well established. For self-affine surfaces the morphology of growing films, however, is often characterized by the correlation length ξ of the height-height correlation and the roughness exponent α governing the behavior at small lateral distances. Recently, it has been emphasized that for unstable growth conditions, characteristic lengths (average pyramid sizes) appear that produce an oscillating character of the height-height correlation. Here we investigate the influence of both kinds of correlations on the diffraction spots. The oscillating correlation causes a splitting of the diffuse shoulder into satellites. The satellite position and half-width show characteristic oscillations depending on the scattering condition. From the latter one can determine the roughness exponent α . The correlation length ξ and the characteristic length can be evaluated from the satellite half-width and position at the out-of-phase scattering condition taking into account the rms height w . This model has been applied to the statistical growth of Ag adlayers on Ag(111) at low temperatures where the satellites of the diffuse shoulder point to the formation of pyramids. From the phase dependence we obtain the roughness exponent $\alpha = \frac{1}{2}$. The step density and the correlation length ξ increase with increasing coverage while no coarsening of the pyramid sizes is observed. [S0163-1829(98)13419-7]

I. INTRODUCTION

There is a steadily increasing interest in studying the epitaxial growth of thin films. On one hand, this great deal of interest is based upon the fact that even on a scale of very few nanometers the perfection of thin films becomes more and more technologically important. On the other hand, from the physicist's point of view the growth of thin films offers the opportunity to study systems far from equilibrium for which a systematic statistical description is not available at the moment.

Several growth modes (layer-by-layer, island, or Stranski-Krastanov growth modes) have been proposed and reported for heteroepitaxial adlayers due to the interplay between interface and surface energies if the growth process is performed close to equilibrium conditions.^{1,2} Applying the same considerations to the growth of homoepitaxial films, one expects that the film grows in the layer-by-layer growth mode so that the film roughness (rms height w) should oscillate with increasing coverage between $w=0$ for the perfectly closed film after depositing an integral number of atomic layers and the maximum roughness $w=d/2$ in between (d denotes the step height). The films, however, are deposited mostly far away from equilibrium conditions so that kinetic effects dominate the morphology. Thus different growth modes such as the multilayer and the random growth mode are observed where the film roughness is between the pure layer-by-layer ($w \leq d/2$) and island growth modes ($w \propto \Theta$) whereas Θ denotes the coverage (average film thickness).³⁻⁵

These kinetic effects on the film growth are an extensively increasing field of investigations. Especially, it has been proposed that the film morphology shows scaling behavior of self-affine surfaces (kinetic roughening): both the rms height w and the correlation length ξ (characterizing the

vertical and lateral roughness, respectively) follow power laws $w \propto \Theta^\beta$ and $\xi \propto \Theta^{1/2}$.⁶ Recently it has been reported that additional barriers at atomic steps (Ehrlich-Schwoebel barrier) cause an uphill diffusion so that the film morphology is unstable since pyramidlike structures and mounds develop.⁷ This growth mode has been studied by Monte Carlo (MC) simulations and Langevin equations and it has been shown that the slope of the pyramids is constant for the long time limit while the average pyramid size follows the scaling law $\langle \Lambda \rangle \propto \Theta^n$.⁸⁻¹² This coarsening of the films has been observed for both semiconductor^{13,14} and metal epitaxy.¹⁵⁻¹⁸

For these investigations, scanning tunneling microscopy (STM) and diffraction techniques such as helium atom scattering (HAS), low-energy electron diffraction (LEED), or reflection high-energy electron diffraction (RHEED) are used mostly. Both techniques probe different properties of surfaces. STM records directly images of the film surface. From these images one has to evaluate the height-height correlation, which can be analyzed with respect to the rms height w , the correlation length ξ , or the average mound size $\langle \Lambda \rangle$. On the other hand, the analysis of diffraction patterns is based directly upon correlation functions such as the pair correlation and the phase correlation. All correlation functions will be defined and explained in more detail in Sec. II. Thus it seems on first sight that the microscopic techniques have large disadvantages compared to diffraction techniques. However, the situation is slightly more complicated because the shape of the diffraction spots is directly related to the scaling parameter's rms height and correlation length only close to the in-phase condition (constructive interference of the beam diffracted at all terraces), where the spot splits into a strong central component and a weak diffuse shoulder.¹⁹ On one hand, at this scattering condition one can easily extract the rms height from the intensity of the central compo-

ment. On the other hand, the diffuse shoulder is mostly so weak that its analysis with respect to the correlation length is difficult.

Diffraction techniques are most sensitive to the lateral surface roughness at the out-of-phase scattering condition where the beam diffracted from adjacent terraces interferes destructively. Therefore, this scattering condition is mostly used to investigate the film morphology *during* growth conditions.²⁰ Here, from the diffuse shoulder one obtains the information about the terrace size distribution.^{21,22} Because of the out-of-phase projection, this analysis is independent of the vertical distribution of layers (which may be characterized by the rms height w).²³ On the other hand, the layer distribution has a large impact on the spot profiles for scattering conditions between in-phase and out-of-phase. At the out-of-phase condition the diffuse scattering shows a single shoulder centered at the center of the Brillouin zone for broad terrace size distributions. On the other hand, the splitting into satellites (characterized by the spot position k_0^{out} and the half-width κ_{out}) is observed for sharp terrace size distributions.^{24,25}

Therefore, there is a demand to combine the information obtained from both techniques, the height-height correlation (parametrized by the correlation length ξ and the characteristic wave vector q_0) and the diffraction analysis (satellite position k_0^{out} and half-width κ_{out} at the out-of-phase condition). Up to now models have been developed only for the limiting case of submonolayer coverages and for surfaces with infinite rms height (implying also an infinite correlation length). In the first case the diffuse shoulder has a constant shape for all scattering conditions.^{26–29} In the second case the spots do not show any central component, rather the shape of the spots depends on the scattering condition.^{27,30}

Assuming that the surface has N exposed layers, it has been shown that the diffuse shoulder consists in principle of $N-1$ independent single shoulders.^{26,27} The deconvolution of the diffuse shoulder with respect to the single contributions is too difficult. From the experimental point of view it is easier to describe the diffuse shoulder by phase-dependent parameters such as the satellite position and half-width. In this study we will evaluate the phase dependence of both for intermediate rough surfaces with $d \ll w \ll \infty$ from the exponentially attenuated oscillating height-height correlation expected for rough surfaces (unstable growth conditions).

For self-affine surfaces with monotonic height-height correlations, Sinha *et al.* have evaluated spot profiles for the diffraction at continuous self-affine surfaces.³¹ Recently, Yang *et al.* have extended the diffraction spot analysis to self-affine surfaces of epitaxial films with monoatomic steps including the periodicity of the spot profiles with respect to the vertical scattering condition K_{\perp} .^{32,33} Their analysis emphasizes that the spot profile half-width at the out-of-phase condition is time invariant if the growth process follows scaling laws.

Figure 1 shows an idealized surface with regularly arranged pyramids. On a mesoscopic scale the pyramids have smooth facets. A closer microscopic view of the facets [circle in Fig. 1(a)], however, shows atomic steps. Both features have impact on the diffraction pattern at different scattering conditions. Close to the in-phase condition ($K_{\perp}^{\text{in}} = 2\pi n/d$), satellites with periodicity $2\pi/\Lambda$ are observed

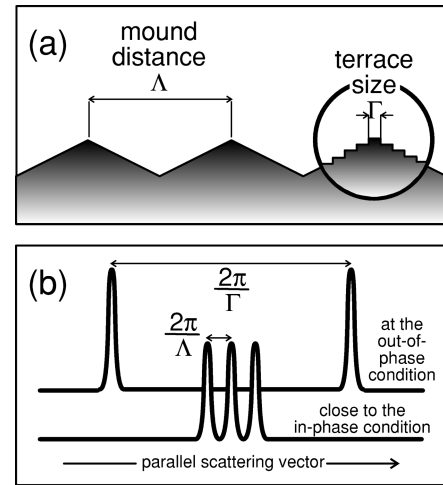


FIG. 1. (a) Schematic drawing of a surface with regular pyramids and (b) the diffraction pattern obtained from it. On a mesoscopic scale the pyramids have smooth sides (facets) that, however, have atomic steps on a microscopic scale (see enlarged area in the circle). Close to the in-phase condition the diffraction pattern is sensitive only to the largest height differences so that one observes the periodicity Λ of the average pyramid-pyramid distance. At the out-of-phase condition the diffraction pattern is only sensitive to the atomic steps so that the step-step distance Γ governs the diffraction pattern.

while the periodicity shifts to $2\pi/\Gamma$ at the out-of-phase condition [$K_{\perp}^{\text{out}} = (2n+1)\pi/d$]. Here Λ and Γ denote the mound-mound distance and the step-step distance, respectively.

Here, the satellites point apparently to oscillating correlation functions instead of the monotonic correlation functions for self-affine surfaces. For realistic growth conditions, however, the arrangement of steps and pyramids will not be so perfect that the diffraction pattern is smeared out and the oscillations of the correlation function are attenuated. Equivalent nonmonotonic height-height correlation functions with a maximum due to the characteristic pyramid distance have been reported assuming that the diffusion across steps is hindered by a Ehrlich-Schwoebel barrier.^{9–12,18}

Therefore, here we present a phenomenological model including also oscillating correlations. One goal is to find *simple* relations for the phase dependence of the diffuse shoulder. It will be demonstrated that the roughness parameter α governing the correlation for short distances can be determined from the phase dependence of the single shoulder or the satellite half-width. This enables us to combine the information from the out-of-phase condition where one has easy experimental access to the diffuse shoulder and the parameters characterizing the height-height correlation. Thus we present a way to determine the basic parameters used for the analysis of different growth models (including pyramidal growth) also from diffraction experiments.

The remainder of this paper is organized as follows. In the next section we define the basic correlation functions necessary for the evaluation of the spot profiles from the height-height correlation. We evaluate the profile of the diffuse shoulder for both nonoscillating and oscillating height-height correlations in Sec. III. In Sec. IV we apply our analysis to Ag films grown on Ag(111) at low temperature. Finally we

discuss our results and compare them with reported investigations.

II. BASIC CORRELATIONS FOR ROUGH SURFACES

One major tool for the morphology analysis of surfaces are correlation functions. In this section we will remind the reader of the definition and the basic properties of those correlation functions mostly used for the morphology analysis. Furthermore, we will present a simple relation between the height-height correlation defined by

$$H(\mathbf{r}) = \langle [h(\mathbf{r}' + \mathbf{r}) - h(\mathbf{r}')]^2 \rangle = \sum_h h^2 d^2 C(\mathbf{r}, h) \quad (1)$$

and the phase correlation upon which the evaluation of diffraction spots is based. The height-height correlation is often used to characterize the surfaces morphology obtained by microscopic techniques or MC simulations. Here $h(\mathbf{r})$ is the height of the surface at the lateral position \mathbf{r} . The brackets $\langle \rangle$ denote averaging with respect to \mathbf{r}' . The last equality of Eq. (1) shows that the height-height correlation can also be evaluated from the pair correlation $C(\mathbf{r}, h)$ (the probability that two surface atoms with lateral distance \mathbf{r} have a height difference of hd , where d denotes the step height and h is an integer).

From Eq. (1) it can be demonstrated that the height-height correlation has the limiting values $H(0)=0$ and $H(\infty) = 2w^2$, where w denotes the rms height (asperity height) defined by $w^2 = \langle h^2(r') \rangle - \langle h(r') \rangle^2$. Therefore, Eq. (1) can also be presented by

$$H(\mathbf{r}) = 2w^2[1 - g(\mathbf{r})] \quad (2)$$

with the autocorrelation $g(\mathbf{r})$ [implying $g(0)=1$ and $g(\infty)=0$].⁶ For self-affine surfaces, the height-height correlation has the asymptotic behavior

$$H(r \ll \xi) \approx 2w^2 \left(\frac{r}{\xi} \right)^{2\alpha} \quad (3)$$

introducing the roughness parameter α . It is related to the exponents β and z presented previously for the scaling laws of self-affine surfaces via $\alpha = z\beta$. To adapt phenomenologically the behavior of $H(r)$ for short and long distances, the autocorrelation

$$g(r) = \exp \left[- \left(\frac{r}{\xi} \right)^{2\alpha} \right] \quad (4)$$

has been proposed and used by different authors.^{31–33}

Figure 2(a) illustrates these properties for $\alpha=0.5$ assuming that $g(r)$ is a monotonically decreasing function ($\xi q_0=0$) as presented in Eq. (4) or is modified by $\cos(q_0 r)$ to mimic oscillating correlations ($\xi q_0=2$).

The analysis of diffraction spots is based upon the lattice factor

$$G(\mathbf{K}) = \int d\mathbf{r} e^{i\mathbf{K}_{\parallel} \cdot \mathbf{r}} \Phi(\mathbf{r}, K_{\perp}), \quad (5)$$

where \mathbf{K}_{\parallel} and K_{\perp} denote the components of the scattering vector \mathbf{K} parallel and perpendicular to the surface, respec-

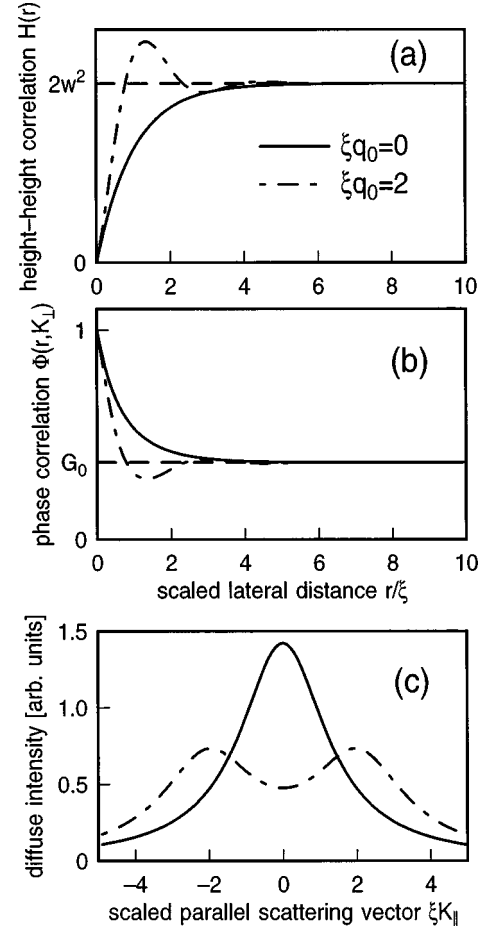


FIG. 2. (a) Schematic drawings for monotonic nonoscillating (solid line) and oscillating (dot-dashed line) height-height correlations. Both start at $H(0)=0$ and approach asymptotically $2w^2$ (dashed line). The oscillating correlation has an overshoot with maximum close to $2\pi/q_0$. (b) Phase correlation for the height-height correlation following Eq. (10) reflecting the nonoscillating (solid line) and oscillating behavior (dot-dashed line), respectively. (c) Diffuse shoulder from Fourier transform of Eq. (10). While the shoulder has its maximum at the center of the Brillouin zone for the nonoscillating correlation (solid line) it splits into satellites for the oscillating correlation (dot-dashed line).

tively. Equation (5) shows that the lattice factor is the two-dimensional Fourier transform of the phase correlation

$$\Phi(\mathbf{r}, K_{\perp}) = \langle e^{iK_{\perp}[h(\mathbf{r}'+\mathbf{r})-h(\mathbf{r}')]} \rangle = \sum_h C(\mathbf{r}, h) e^{iK_{\perp}hd}, \quad (6)$$

where the brackets $\langle \rangle$ denote again averaging with respect to \mathbf{r}' . The spot profiles split into a diffuse shoulder and a sharp δ -function-like central component with intensity $G_0(K_{\perp})$ for surfaces with finite rms height w .^{26,34} Therefore, the phase correlation has the limits $\Phi(\infty, K_{\perp}) = G_0(K_{\perp})$ and $\Phi(0, K_{\perp}) = 1$ so that Eq. (6) can be rearranged to

$$\Phi(\mathbf{r}, K_{\perp}) = G_0(K_{\perp}) + [1 - G_0(K_{\perp})] \varphi(\mathbf{r}, K_{\perp}). \quad (7)$$

Here $\varphi(\mathbf{r}, K_{\perp})$ is the two-dimensional Fourier transform of the diffuse shoulder. Figure 2(b) shows the phase correlation functions for the monotonic and the oscillating height-height correlation from Fig. 2(a) at the out-of-phase condi-

tion. While the shoulder is a single Lorentzian centered at K_{\parallel} for the monotonic height-height correlation, the line scan splits into two satellites for the oscillating correlation [see Fig. 2(c)].

Comparing Eq. (1) and Eq. (6) shows that the height-height correlation cannot be transformed into the phase correlation in a simple way except by use of the pair correlation. Therefore, in many studies one assumes a special (more or less realistic) *vertical* dependence of $C(\mathbf{r}, h)$ on h , e.g., a Gaussian form $C(\mathbf{r}, h) = \exp[-h^2/\lambda(\mathbf{r})]/\sqrt{2\pi\lambda(\mathbf{r})}$. This ansatz, however, has the disadvantage that one does not obtain a closed-form analytic relation between the height-height correlation and the phase correlation.³³

Therefore, we assume here that the pair correlation can be described by the convolution

$$C(\mathbf{r}, h) = \sum_l p(\mathbf{r}, h+l)p(\mathbf{r}, l). \quad (8)$$

The functions $p(\mathbf{r}, h)$ introduced here can be interpreted easily for $r \rightarrow \infty$: in this limit they denote the distribution of exposed layers. On the other hand, they must have the form $p(\mathbf{r}, h) = \delta_{h,0}$ (Kronecker symbol) for $\mathbf{r} = \mathbf{0}$. For the Gaussian pair correlation described above, the $p(\mathbf{r}, h)$ are also Gaussians with $\lambda(0) = 0$ and $\lambda(\infty) = w/d$.

Often, however, the distribution of exposed layers is not governed by a Gaussian but by an asymmetric distribution.¹² Since a Poisson distribution of exposed layers is reported often from experiments, we assume also a Poisson shape:

$$p(\mathbf{r}, h) = \frac{\lambda^h(\mathbf{r})}{h!} e^{-\lambda(\mathbf{r})}. \quad (9)$$

Since this implies $H(\mathbf{r}) = 2\lambda(\mathbf{r})$, we obtain the simple analytic relation

$$\begin{aligned} \Phi(\mathbf{r}, K_{\perp}) &= \exp[-2H(\mathbf{r})(1 - \cos K_{\perp}d)] \\ &= \exp\{-\eta(K_{\perp})[1 - g(\mathbf{r})]\} \end{aligned} \quad (10)$$

between the height-height correlation and the phase correlation. The scattering condition enters via $\eta(K_{\perp}) = 2(w^2/d^2)(1 - \cos K_{\perp}d)$ including the rms height w . Since this expression will be the basic parameter for our studies, we denote it as a *combined scattering condition*. A similar relation has also been proposed by Villain *et al.* for vicinal surfaces.³⁵

The central component has the intensity

$$G_0(K_{\perp}) = \exp\left[-2\frac{w^2}{d^2}(1 - \cos K_{\perp}d)\right] \quad (11)$$

due to the Poisson distribution of exposed layers.³⁶ Finally, we would like to mention that the Poisson statistics does not automatically mean that the rough surface is produced by the statistical growth mode. This growth mode is characterized additionally by $w/d = \sqrt{\Theta}$ while we do not apply any restrictions to the relation between rms height and coverage.

It has been shown that the simple relation $\varphi(\mathbf{r}, K_{\perp} \approx K_{\perp}^{\text{in}}) \approx g(\mathbf{r})$ is valid for scattering conditions close to the in-phase condition $\Delta K_{\perp} = K_{\perp} - K_{\perp}^{\text{in}} \ll 2\pi/d$ approximating the exponential of Eq. (10) by the first order Taylor approximation.¹⁹

Thus for these scattering conditions the phase correlation can be transformed directly to the height-height correlation. This procedure, however, is difficult since the intensity is very weak for this scattering condition. Therefore, there are large experimental errors to determine the height-height correlation. Since the diffuse scattering dominates the spot profile at the out-of-phase condition, we will develop in the following how this information can be used to evaluate the height-height correlation.

III. EVALUATION OF THE DIFFUSE SHOULDER

In diffraction experiments during the early stages of multilayer growth one often observes isotropic diffuse shoulders of the diffraction spots with single Lorentzian or ring-like profiles. Sometimes also broadened satellites close to the fundamental spots are reported where both the half-width and the position of the satellites depend on the scattering condition.^{4,17,18,37-39}

The isotropy of the diffuse scattering implies that also the phase correlation is isotropic. Therefore, for Lorentzian ring-like shoulders the phase correlation $\varphi(r, K_{\perp})$ can be approximated well by the ‘‘experimental’’ phase correlation $\varphi_{\text{exp}}(r, K_{\perp})$ defined by

$$\varphi_{\text{exp}}(r, K_{\perp}) = e^{-\kappa r} \cos(k_0 r) \quad (12)$$

with $r = |\mathbf{r}|$, where both parameters $\kappa = \kappa(K_{\perp})$ and $k_0 = k_0(K_{\perp})$ depend on the scattering condition and the surface roughness. Consequently, we obtain the phase correlation

$$\Phi_{\text{exp}}(r, K_{\perp}) = G_0(K_{\perp}) + [1 - G_0(K_{\perp})]e^{-\kappa r} \cos(k_0 r). \quad (13)$$

This exponentially attenuated oscillating shape of the diffuse shoulder has also been confirmed evaluating the spot profile for sharp terrace size distributions assuming that the size of the adjacent terraces are not correlated. Both spot profile parameters can be interpreted easily for the out-of-phase scattering condition.²⁵

$$\kappa_{\text{out}} = \kappa(K_{\perp}^{\text{out}}) \approx \frac{\pi^2}{2\langle\Gamma\rangle} \left(\frac{\sigma}{\langle\Gamma\rangle}\right)^2 \quad (14)$$

and

$$k_0^{\text{out}} = k_0(K_{\perp}^{\text{out}}) \approx \frac{\pi}{\langle\Gamma\rangle} \left[1 - \frac{\pi^2}{6} \left(\frac{\sigma}{\langle\Gamma\rangle}\right)^4\right], \quad (15)$$

where $\langle\Gamma\rangle$ and σ denote the average terrace size and the standard deviation of the terrace size distribution, respectively.

The attenuated oscillation of the phase correlation implies that also the pair correlation shows equivalent oscillations. Therefore, we modify the autocorrelation of Eq. (4) by

$$g(r) = \exp\left[-\left(\frac{r}{\xi}\right)^{2\alpha}\right] \cos(q_0 r) \quad (16)$$

to include these oscillations. We obtain the height-height correlation

$$H(r) = 2w^2[1 - e^{-(r/\xi)^{2\alpha}} \cos(q_0 r)] \quad (17)$$

and the phase correlation

$$\Phi(r, K_{\perp}) = \exp\{-\eta(K_{\perp})[1 - e^{-(r/\xi)^{2\alpha}} \cos(q_0 r)]\}. \quad (18)$$

This simple model shows the main features reported for surfaces with mounds: the asymptotic behavior $H(r \ll \xi) \propto (r/\xi)^{2\alpha}$ and a maximum of the height-height correlation.^{9,10}

The parameter q_0 causes the height-height correlation to oscillate. Following our previous discussion of Fig. 1, this implies that the characteristic wave vector is related to the characteristic length (average pyramid size $\langle \Lambda \rangle$) via $q_0 = 2\pi/\langle \Lambda \rangle$. Such oscillations of the height-height correlation have been observed in different MC simulations of epitaxial growth including an Ehrlich-Schwoebel barrier.^{9,11,12,18}

We would like to remark that the parameters ξ and q_0 depend exclusively on the morphology while the diffraction parameters $\kappa(K_{\perp})$ and $k_0(K_{\perp})$ include explicitly the scattering condition. Therefore, we will study in the following how the morphology parameters determine these diffraction parameters. For this purpose we will compare the exactly evaluated phase correlation $\Phi(r, K_{\perp})$ of Eq. (18) with the approximated phase correlation $\Phi_{\text{exp}}(r, K_{\perp})$ of Eq. (13) for different combined scattering conditions $\eta(K_{\perp}) = 2(w^2/d^2)(1 - \cos K_{\perp}d)$ (including the rms height w of the surface), correlation lengths ξ , and characteristic wave vectors q_0 .

Figure 3 shows the results having fitted the phase correlations calculated by Eq. (18) (open symbols) for roughness exponent $\alpha = 0.5$ to the approximation (solid line) following Eq. (13) for different periodicities ξq_0 and combined scattering conditions $\eta(K_{\perp})$. Obviously the agreement between the approximation motivated by the experimental results and the exact shape is excellent.

A. Nonoscillating correlations

The open symbols of Fig. 4 show the scaled half-width $\xi\kappa(K_{\perp})$ obtained from fitting the phase correlation of Eq. (18) for $\xi q_0 = 0$ with the approximated phase correlation of Eq. (13) for different α . For this analysis we used the fitting range $0 \leq r \leq 10\xi$. As expected, one obtains the asymptotic behavior $\xi\kappa(K_{\perp}) \approx 1$ for $\eta(K_{\perp}) \ll 1$. On the other hand, the scaled half-width increases drastically for the opposite case. The linear slope of the log-log plot demonstrates that the half-width follows a power law for large $\eta(K_{\perp}) \gg 1$ with crossover to the constant half-width at $\eta(K_{\perp}) \approx 1$. The exponent of the power law depends on the roughness exponent α .

The only adjustable parameter of Eq. (13) is the half-width $\kappa(K_{\perp})$ since the rms roughness w and the scattering condition K_{\perp} fix the value of the phase correlation for infinite lateral distance to $G_0 = e^{-\eta(K_{\perp})} = e^{-2(w^2/d^2)(1 - \cos K_{\perp}d)}$. A proper way to obtain $\kappa(K_{\perp})$ is to require that both the approximation form of Eq. (13) and the exact form of Eq. (18) must be identical for $r = \kappa^{-1}$ [where we have $\varphi_{\text{exp}}(\kappa^{-1}) = e^{-1}$]. Thus we have the criterion

$$\Phi(\kappa^{-1}, K_{\perp}) = \Phi_{\text{exp}}(\kappa^{-1}, K_{\perp}) \quad (19)$$

which can only be fulfilled for

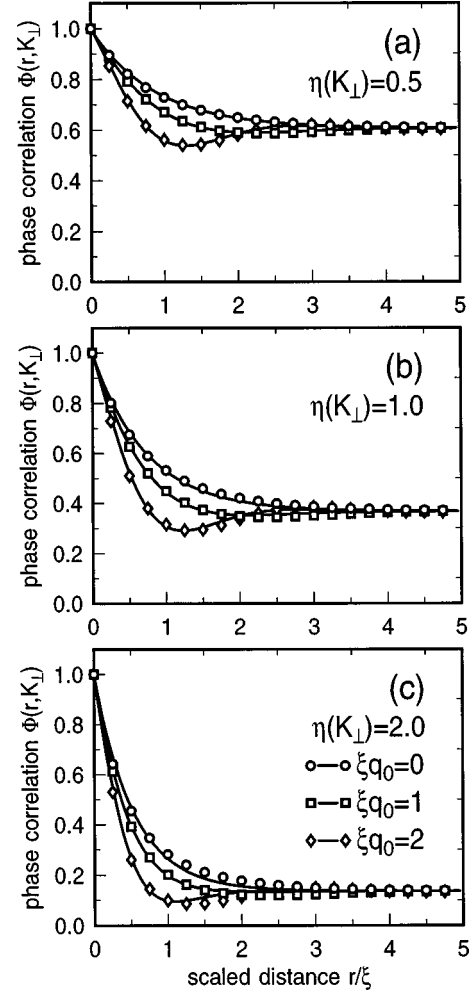


FIG. 3. Comparison of the phase correlation evaluated from Eq. (17) (open symbols) and the least square fit following Eq. (18) for different scattering conditions (a) $\eta(K_{\perp}) = 0.5$, (b) $\eta(K_{\perp}) = 1$, (c) $\eta(K_{\perp}) = 2$ and scaled characteristic wave vectors ξq_0 . The definition of the symbols shown in (c) applies also to (a) and (b).

$$\xi\kappa(K_{\perp}) = [\ln \eta(K_{\perp}) - \ln \ln(1 - e^{-1} + e^{\eta(K_{\perp}) - 1})]^{-1/2\alpha}. \quad (20)$$

The solid lines of Fig. 4 demonstrate that the predicted behavior of Eq. (20) follows exactly the fitting result for the whole investigated range of $\eta(K_{\perp})$. Equation (20) has the asymptotic behavior $\xi\kappa(K_{\perp}) \approx 1$ for $\eta(K_{\perp}) \ll 1$ and $\xi\kappa(K_{\perp}) \approx [\eta(K_{\perp})]^{1/2\alpha}$ for $\eta(K_{\perp}) \gg 1$.

Equation (20), however, is quite complicated to describe the approximated phase dependence of the half-width. Therefore, from the practical point of view, it is desirable to simplify Eq. (20) by a phenomenological relation describing exactly the same asymptotic behavior. The dashed line in Fig. 4 demonstrates that

$$\xi\kappa(K_{\perp}) = \left[\frac{\eta(K_{\perp})}{1 - e^{-\eta(K_{\perp})}} \right]^{1/2\alpha} = \left[\frac{2(w^2/d^2)(1 - \cos K_{\perp}d)}{1 - e^{-2(w^2/d^2)(1 - \cos K_{\perp}d)}} \right]^{1/2\alpha} \quad (21)$$

fulfills excellently this demand so that we base the following considerations on this result.

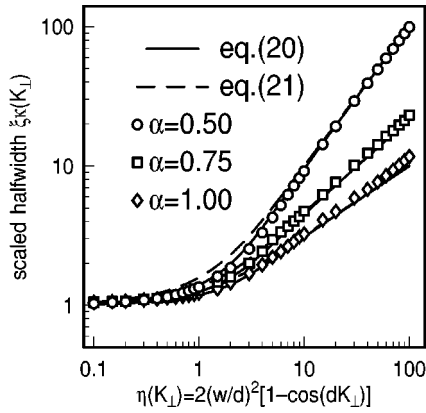


FIG. 4. Dependence of the diffraction spot half-width (scaled with respect to the correlation length ξ) on the combined scattering condition $\eta(K_{\perp})$. The open symbols are obtained from fitting the ‘‘exact’’ phase dependence of Eq. (18) with the ‘‘experimental’’ phase correlation Eq. (13). While both are identical for small scattering conditions, they show a different behavior for large scattering conditions. Additionally, the comparison of the fitting result with Eq. (20) and Eq. (21) is shown. The agreement is excellent.

Of course the main goal of this analysis is to study how the surface morphology influences the diffuse scattering for different scattering conditions. Therefore, Fig. 5 shows the phase dependence of the scaled half-width $\xi\kappa(K_{\perp})$ of the diffuse shoulder for different rough surfaces (roughness exponent $\alpha=0.5$). The open dots are again the result of the fitting procedure described before, while the solid lines are obtained from Eq. (21). Obviously the agreement is always excellent for rough surfaces while Eq. (21) overestimates the half-width for smooth surfaces.

This, in fact, is an inherent feature of our model due to the assumed vertical dependence of the pair correlation. Thus, for instance, our model cannot be applied well to the growth morphology in the submonolayer range implying a two-level

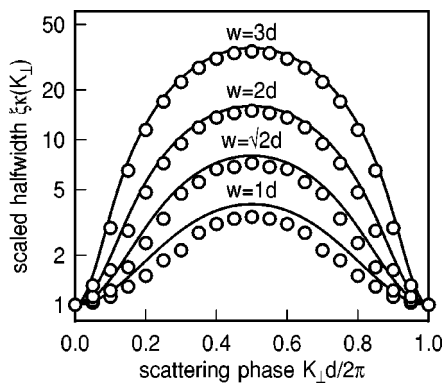


FIG. 5. Dependence of the scaled half-width on the scattering phase $dK_{\perp}/2\pi$ for roughness exponent $\alpha=0.5$ and constant correlation length ξ but varying the rms height w . The solid lines show the predicted dependence from Eq. (21) while the open dots are from the fitting procedure. In contrast to the scattering close to the in-phase condition, where the half-width does not depend on the rms roughness or the scattering condition, the half-width increases drastically close to the out-of-phase condition with increasing rms roughness. Note the logarithmic scale. The agreement between Eq. (21) and the exactly evaluated half-width increases with increasing rms roughness w .

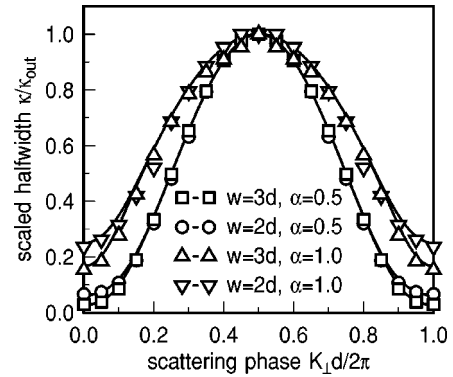


FIG. 6. Comparison of the half-width for different roughness exponents ($\alpha=0.5$ and $\alpha=1.0$) and constant half-width at the out-of-phase condition. The open symbols are obtained from the fitting procedure and the solid lines show the behavior predicted by Eq. (21). The phase dependence is smoother for larger roughness exponents. Equivalent to the result illustrated by Fig. 5, the half-width at the in-phase condition increases with decreasing rms roughness w .

roughness (substrate and islands). It is well known that for this surface the shape of the diffuse shoulder does not depend on the scattering condition. It has the constant value $\kappa=\xi^{-1}$.^{19,26} Therefore, our model overestimates the half-width close to the out-of-phase condition for too smooth surfaces.

The roughness parameter α influences also the phase dependence of the half-width close to the out-of-phase scattering condition due to the power law for large $\eta(K_{\perp})$. Comparing the phase dependence for $\alpha=0.5$ and $\alpha=1.0$, Fig. 6 illustrates the influence of the rms height. Here the half-width at the out-of-phase condition is identical for all curves implying that the step density is identical. Again the open symbols are obtained from the fitting analysis and the solid lines from the phenomenological Eq. (21). The agreement is perfect so that Eq. (21) can be considered as well established to describe the phase dependence for surfaces with different roughness parameters α . Figure 6 demonstrates that the phase dependence becomes smoother for $\alpha=1$ so that the ratio between out-of-phase half-width and in-phase half-width increases. Therefore the phase dependence of the half-width offers the possibility to determine the roughness parameter α .

We have just described how the phase dependence of the half-width can be concluded from Eq. (21). However, one can also interpret this relation with respect to different roughness parameters for the out-of-phase condition:

$$\kappa_{\text{out}} = \kappa(K_{\perp}^{\text{out}}) = \frac{(2w/d)^{1/\alpha}}{\xi}. \quad (22)$$

It has been shown for $\alpha=0.5$ (Lorentzian shoulder due to a geometric terrace size distribution) that the half-width at the out-of-phase condition depends on the step density $\rho=1/\langle\Gamma\rangle$ via $\kappa_{\text{out}}=2\rho$.⁴⁰ Assuming that the half-width is purely determined by the step density, Eq. (22) can be interpreted as

$$\rho = \frac{(2w/d)^{1/\alpha}}{2\xi}. \quad (23)$$

Yang *et al.* have reported a similar relation.^{32,33} Additionally, they pointed out that the half-width is invariant for the self-affine surfaces of thick films due to the scaling relations $w \propto \Theta^\beta$ and $\xi \propto \Theta^{\beta/\alpha}$.

B. Oscillating correlations

After the analysis of pure exponential correlation functions, we extend our study to the oscillating correlation functions of Eq. (16) with some preferential characteristic wave vector $\xi q_0 > 0$. Therefore, the second parameter $k_0(K_\perp)$ is introduced to solve the approximation problem to fit Eq. (13) to the exact form of Eq. (18).

Because of the former consideration concerning the equivalence of the height-height correlation and the phase correlation for scattering conditions close to the in-phase condition, it is clear that $\kappa(K_\perp) = \xi^{-1}$ and $k_0(K_\perp) = q_0$ for $\eta(K_\perp) < 1$ (equivalent to $|K_\perp - K_\perp^{\text{in}}| < w^{-1}$). Thus we will proceed studying the other asymptotic behavior for $\eta(K_\perp) \gg 1$.

In this case of large rms height w with scattering conditions not too close to the in-phase condition, we concentrate our analysis on small lateral distances since the phase correlation vanishes for $r \gg \xi$. We substitute the height-height correlation in Eq. (18) by its asymptotic form so that we obtain

$$\Phi(r, K_\perp) \approx \exp \left[-\eta(K_\perp) \left(\frac{r}{\xi} \right)^{2\alpha} - \eta(K_\perp) \frac{q_0^2}{2} r^2 \right]. \quad (24)$$

Equivalently, the ‘‘experimental’’ phase correlation can be approximated by

$$\Phi_{\text{exp}}(r, K_\perp) \approx \exp \left[-\kappa(K_\perp) r - \frac{1}{2} k_0^2(K_\perp) r^2 \right] \quad (25)$$

since $G_0(K_\perp) \ll 1$. Here we have approximated additionally the cosine of Eq. (13) by the equivalent Gaussian $\cos k_0 r \approx \exp[-\frac{1}{2} k_0^2 r^2]$ valid for $r < q_0^{-1}$ so that Eq. (25) can be compared directly with Eq. (24).

Applying the matching criterion $\Phi(\kappa^{-1}, K_\perp) = \Phi_{\text{exp}}(\kappa^{-1}, K_\perp)$ of Eq. (19) does not lead to a clear result since we have to determine two parameters for the diffraction spot. Therefore, we propose that the linear and the quadratic term of $\Phi_{\text{exp}}(\kappa^{-1}, K_\perp)$ may be adjusted independently to the terms $\propto r^{2\alpha}$ and $\propto r^2$ of $\Phi(\kappa^{-1}, K_\perp)$ so that we obtain

$$\xi \kappa(K_\perp) = [\eta(K_\perp)]^{1/2\alpha} \quad (26)$$

and

$$k_0(K_\perp) = q_0 \sqrt{\eta(K_\perp)}. \quad (27)$$

Equation (26) is identical to the asymptotic behavior of the half-width for nonoscillating correlations. Surprisingly, the roughness exponent α does not have any impact on the relation between the satellite position and the characteristic wave vector.

Equivalent to the examination of the nonoscillating correlations, we proved the validity of Eq. (26) and Eq. (27) fitting the ‘‘experimental’’ phase correlation $\Phi_{\text{exp}}(r, K_\perp)$ to $\Phi(r, K_\perp)$ in the range $0 \leq r \leq 10\xi$. Figure 7 shows the results obtained for $\xi q_0 = 2$ and different roughness exponents α . For $\eta(K_\perp) > 3$, the $\eta(K_\perp)$ dependence of Eq. (26) fits ex-

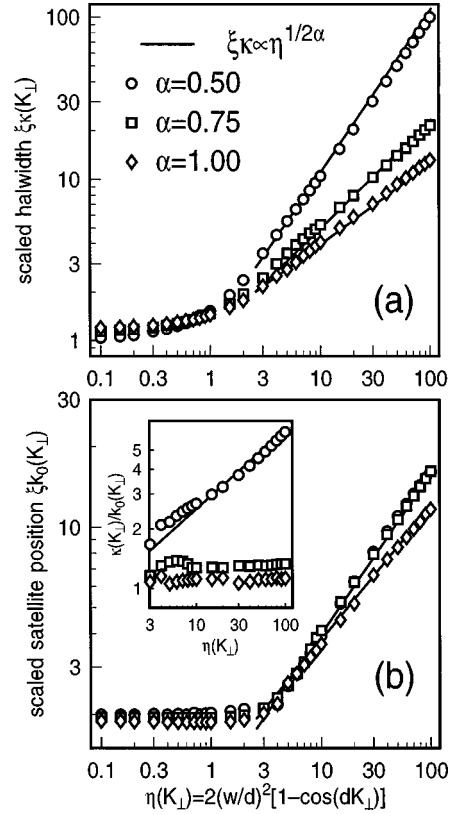


FIG. 7. Dependence of the satellite (a) half-width and (b) position on the scattering condition for rough surfaces with oscillating correlations. The half-width follows the power law $\xi \kappa(K_\perp) \propto [\eta(K_\perp)]^{1/2\alpha}$ as the solid lines show. For the satellite position one obtains $k_0(K_\perp) \propto [\eta(K_\perp)]^x$ (with $x = 0.5 - 0.6$). The inset of (b) shows the dependence of the ratio from satellite half-width and position on the scattering condition. Only for $\alpha = 0.5$ does one obtain a nonconstant dependence.

cellently the behavior of the half-width κ for all roughness exponents. In contrast to Eq. (27), the satellite position does not scale exactly with $\sqrt{\eta(K_\perp)}$ but we obtain exponents from 0.5 to 0.6 [solid lines in Fig. 7(b)].

Figure 8 presents the phase dependence of the satellite position and half-width for rough surfaces with exponent $\alpha = 0.5$ and constant correlation length ξ . Here the open dots are the data obtained from the fitting procedure (equivalent to Fig. 7).

These results are compared to the phenomenological equations

$$\xi \kappa(K_\perp) = \left[\frac{\eta(K_\perp)}{1 - e^{-\eta(K_\perp)}} \right]^{1/2\alpha} \quad (28)$$

and

$$k_0(K_\perp) = q_0 \sqrt{\frac{\eta(K_\perp)}{1 - e^{-\eta(K_\perp)}}} \quad (29)$$

adapted from Eq. (21).

The solid lines in Fig. 8 show that the agreement is excellent for rough surfaces ($w \geq 2d$). Obviously the satellite

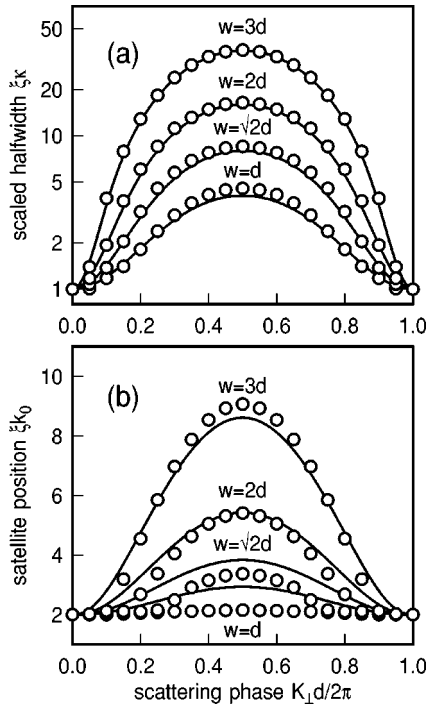


FIG. 8. Phase dependence of both the satellite (a) half-width (note the logarithmic scale) and (b) position for $\alpha=0.5$, $\xi q_0=2$ and different rms roughness w . The phase dependence of the satellite half-width is described excellently by Eq. (21) as the solid line shows. For the satellite position there are deviations for smooth surfaces $w < 2d$.

position is overestimated by Eq. (29) for smoother surfaces while the dependence of the half-width Eq. (28) still fits well.

Figure 9 shows the impact of the roughness parameter on the phase dependence of the spot profile parameters $\xi\kappa$ and ξk_0 for a surface with characteristic wave vector $\xi q_0=2$. Here, we assumed an identical half-width and position for all curves at the out-of-phase condition. As mentioned before, this is equivalent to identical terrace size distributions. Figure 9(a) shows that the dependence of the satellite half-width becomes smoother with increasing roughness exponent so that the value at the in-phase condition increases more drastically with respect to the exponent than to the rms roughness w . On the other hand, Fig. 9(b) demonstrates that the behavior for the satellite position is vice versa. Here the roughness exponent has almost no impact on the curve. Even the rms roughness does not change the behavior drastically except for scattering conditions close to the in-phase condition where the curves have the asymptotic value $k_0^{\text{in}}/k_0^{\text{out}}=d/2w$.

Finally we would like to discuss the relation between the characteristic parameters ξ and q_0 of the height-height correlation and the diffraction parameters κ_{out} and k_0^{out} at the out-of-phase condition. On one hand, we can directly use Eq. (22) since Eq. (26) is identical to the equivalent relation for nonoscillating correlations. On the other hand, we obtain for the characteristic wave vector

$$k_0^{\text{out}} = k_0(K_{\perp}^{\text{out}}) = 2 \frac{w}{d} q_0. \quad (30)$$

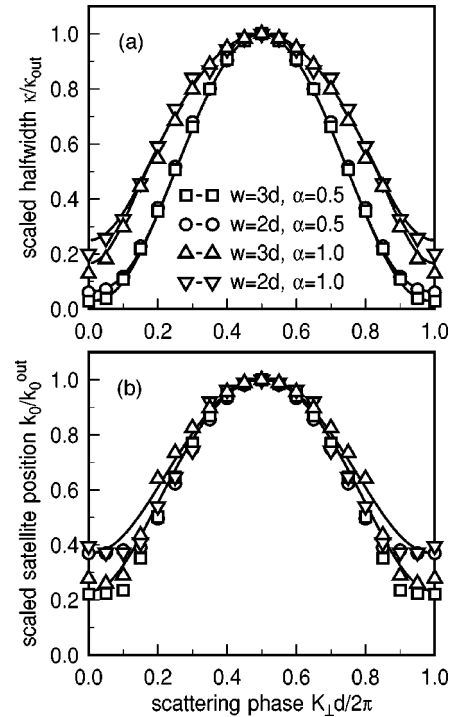


FIG. 9. Impact of the roughness exponent $\alpha=1.0$ and $\alpha=0.5$ (characteristic wave vector $\xi q_0=2$) on the phase dependence of the satellite (a) half-width and (b) position with identical spot parameters at the out-of-phase condition. The definition of the symbols in (a) applies also to (b). The phase dependence of the half-width is governed by the roughness exponent since the rms roughness w does not change the behavior drastically. For $\alpha=1.0$ the dependence is much flatter than for $\alpha=0.5$. The phase dependence of the satellite position is only influenced by the rms roughness (solid lines for $w/d=2$ and $w/d=3$, respectively).

Although we recover Eq. (26) for the same relation between half-width and correlation length as for the nonoscillating correlations, here the interpretation is different. For the self-affine surfaces the half-width of the shoulder is related to the step density [cf. Eq. (23)]. Earlier we reported [cf. Eq. (15)] that the satellite position is determined by the average terrace size sharp distributions. Therefore, we obtain the step density via

$$\rho = \frac{1}{\langle \Gamma \rangle} = \frac{2w}{\pi d} q_0 \quad (31)$$

neglecting the term $\propto \sigma^4 / \langle \Gamma \rangle^4$ of Eq. (15).

IV. APPLICATION TO THE EPITAXIAL GROWTH OF Ag ON Ag(111) AT LOW TEMPERATURE

In the following we will apply the diffraction analysis presented in the preceding section to characterize rough Ag films grown on Ag(111) at 130 K. The Ag film was deposited on a 100-ML-thick Ag template layer that has been grown on a Si(111) 7×7 sample. Spot profiles of the specular beam were measured with a high-resolution low-energy electron diffraction instrument with a transfer width of 100 nm. The experimental results concerning the growth mode and the annealing behavior of the Ag film have been published previously.³⁹ Here we would like to concentrate our

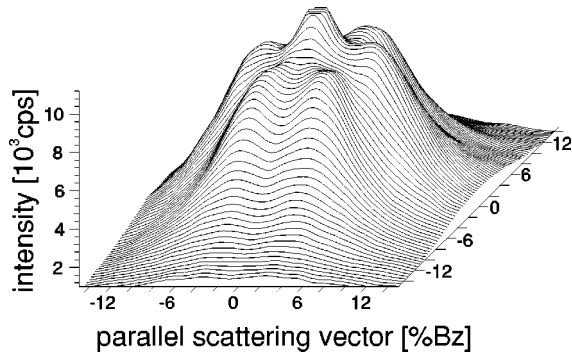


FIG. 10. Contour plot of the (00) spot recorded at the out-of-phase condition $K_{\perp} d/2\pi = 2.5$ after deposition of 2.5 ML Ag. The diffuse shoulder shows six satellites pointing to a sharp terrace size distribution. We used a cutoff for the central component to emphasize the diffuse satellites.

analysis on the comparison of the experimental data with the theoretical approach for the diffraction from surfaces with oscillating correlations developed here.

Figure 10 shows a contour plot of the specular (00) beam recorded at the out-of-phase condition $K_{\perp} d/2\pi = 2.5$ from a 2.5 ML Ag film. Clearly one can distinguish six satellites at a distance of $k_0 = 5\%$ Bz from the central component. Since we do not observe a single Lorentzian shoulder, rather satellites, the terrace size distribution cannot be a geometric distribution. It must be sharper implying $\sigma < \langle \Gamma \rangle$. We have observed this effect for the total investigated coverage range $0.5 \text{ ML} \leq \Theta \leq 3.5 \text{ ML}$ as Fig. 11 demonstrates. Figure 11(a) presents the half-width κ_{out} and the position k_0^{out} at the out-of-phase condition. Both increase with increasing coverage following the power law $\Theta^{2/3}$ (solid and dashed line, respec-

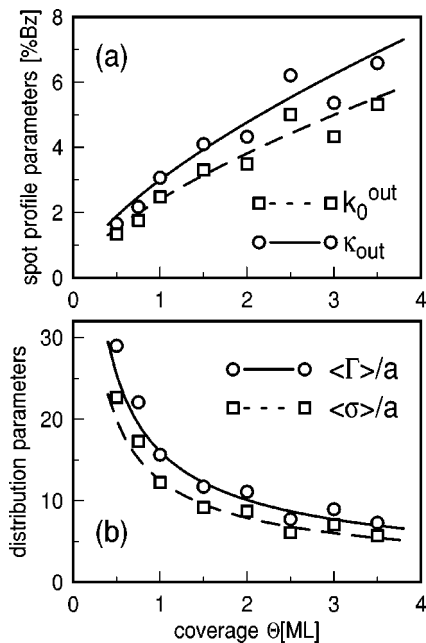


FIG. 11. (a) Coverage dependence of the satellite position k_0^{out} and half-width κ_{out} . Both follow the power law $\Theta^{2/3}$ (dashed and solid line, respectively). (b) Coverage dependence of the average terrace size $\langle \Gamma \rangle$ and the standard deviation σ of the terrace size distribution. Both scale with increasing coverage so that they follow the power law $\Theta^{-2/3}$.

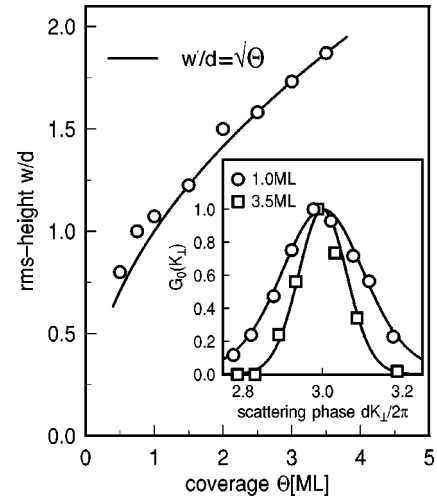


FIG. 12. Coverage dependence of the rms height w obtained from the analysis of the central component intensity. The rms roughness follows the power law $\Theta^{1/2}$ pointing to a statistical growth (Poisson growth) of the Ag adlayer without interlayer transport. The inset shows the phase dependence of the scaled central component intensity $G_0(K_{\perp})$ for $\Theta = 1.0 \text{ ML}$ and $\Theta = 3.5 \text{ ML}$. The solid lines are least square fits of Eq. (11) to the experimental data from which one obtains the rms height w .

tively). As described previously,²⁵ this kind of diffuse spot profile can be analyzed with respect to the average terrace size and the standard deviation of the terrace size distribution. The result is shown in Fig. 11(b). According to the power law for the spot profile parameters κ_{out} and k_0^{out} , we find that both $\langle \Gamma \rangle$ and σ follow the power law $\Theta^{-2/3}$. Thus the terrace size distribution obeys a scaling law: it does not become broader or sharper with increasing coverage but scales with the average terrace size.

The main goal of this study, however, is to describe not only the effect of the oscillating correlations during the earlier stages of epitaxy on the diffraction pattern at the out-of-phase condition, but to extend the analysis to *all* scattering conditions. Therefore, we have analyzed spot profiles recorded for scattering conditions $2.5 \leq K_{\perp} d/2\pi \leq 3.5$, which show always the typical splitting into a sharp central component and a diffuse isotropic ringlike shoulder for low coverages or a sixfold shoulder with satellites at larger coverages. The diffuse shoulder vanishes at the in-phase condition, which proves that it is caused by atomic steps.

Figure 12 presents the spot profile analysis with respect to the rms height w . For all investigated coverages the scaled central spot intensity $G_0(K_{\perp})$ follows Eq. (11) obtained for a Poisson distribution of exposed layers (solid lines in the inset of Fig. 12). Since $G_0(K_{\perp})$ becomes sharper with increasing coverage, the rms roughness increases. The detailed analysis demonstrates that the rms roughness follows $w = d\sqrt{\Theta}$ (solid line). From this behavior one can conclude that the interlayer diffusion of the deposited Ag is prohibited, obviously due to a Schwoebel barrier at the step edges. For a pure statistical growth without any diffusion, we expect a much smaller average terrace size than observed in Fig. 11. Therefore, we conclude that the intralayer diffusion on terraces cannot be neglected.

The analysis of the diffuse shoulder with respect to the

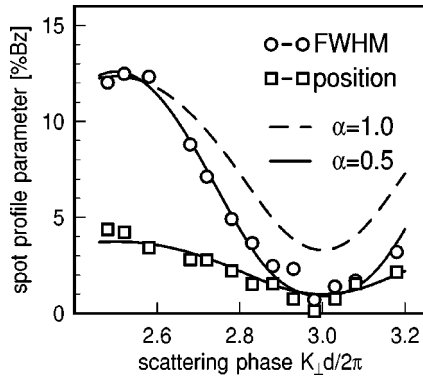


FIG. 13. Phase dependence of the satellite full width at half maximum (FWHM) and position for $\Theta = 3.5$ ML. The solid and dashed lines are the expected phase dependence for roughness exponents $\alpha = 0.5$ and $\alpha = 1.0$, respectively, following Eq. (28). Since the rms roughness can be used as input, the only matching parameter is the FWHM at the out-of-phase condition. Equivalently, Eq. (29) has been used to fit the satellite position (second lower solid line).

position k_0 and the half-width κ of the satellites at various scattering conditions is presented in Fig. 13 for $\Theta = 3.5$ ML. Since the rms roughness of the film has been determined independently from the central component intensity, the only fitting parameter for the phase dependence of the satellite half-width is the roughness exponent α . Comparing the predicted phase dependence for $\alpha = 0.5$ (solid line) and $\alpha = 1.0$ (dashed line) we conclude that the roughness is governed by the exponent $\alpha = 0.5$.

Having determined the roughness exponent $\alpha = 0.5$ from the phase dependence, one can simply evaluate the correlation length of the surface combining the rms roughness w (obtained from the analysis of the central component intensity) and the satellite half-width at the out-of-phase condition following Eq. (22). The result of this evaluation is presented in Fig. 14(a), where the dots are obtained from the evaluation from the experimental results while the solid line shows the relation combining the power laws for the rms roughness ($w \propto \Theta^{1/2}$) and the spot half-width ($\kappa_{\text{out}} \propto \Theta^{2/3}$). Therefore, we obtain again a power law for the correlation length ($\xi \propto \Theta^{1/3}$). Equivalently the characteristic wave vector q_0 can be evaluated from Eq. (30). It follows the power law $q_0 \propto \Theta^{1/6}$. Therefore, we do not observe a strong coarsening of the pyramids. Their size is almost constant.

V. DISCUSSION AND CONCLUSION

On one hand, one goal of the study presented here was to develop a *phenomenological* theory for the diffraction from multilevel surfaces with intermediate rms height. On the other hand, we demonstrated that this model can be applied to investigate both self-affine and non-self-affine surfaces (characterized by the correlation length ξ and the characteristic wave vector q_0) from spot profiles recorded at the out-of-phase condition (characterized by the satellite position k_0 and half-width κ).

For this purpose we evaluated spot profiles for oscillating and nonoscillating correlations. Assuming a Poisson-like vertical (h) dependence of the pair correlation $C(\mathbf{r}, h)$ we

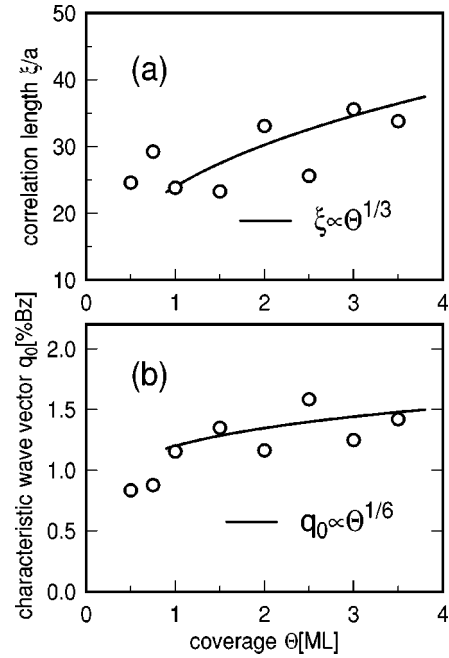


FIG. 14. Evaluation of the coverage dependence of (a) the correlation length ξ and (b) the characteristic wave vector q_0 from the satellite parameters at the out-of-phase condition. The correlation length ξ and the characteristic wave vector q_0 increase following the power laws $\Theta^{1/3}$ and $\Theta^{1/6}$, respectively (solid lines).

obtain simple analytic relations for both the satellite position and the half-width on the scattering conditions with minimum at the in-phase condition ($\kappa_{\text{in}} = \xi^{-1}$ and $k_0^{\text{in}} = q_0$) and maximum at the out-of-phase condition [$\kappa_{\text{out}} = (2w/d)^{1/\alpha}/\xi$ and $k_0^{\text{out}} = 2wq_0/d$].

The diffraction spots from surfaces with submonolayer adlayers split into a sharp central component and a diffuse shoulder with constant half-width. The intensities of both depend on the scattering condition with maximum intensity of the sharp central component at the in-phase condition and minimum intensity at the out-of-phase condition. The phase dependence changes drastically for infinite rough surfaces ($w = \infty$). For these surfaces the spots do not show any central component, rather the spots are broadened and the profiles depend on the scattering condition. Assuming that the sizes of adjacent terraces are not correlated, the spots have Lorentzian profiles with half-width $\kappa(K_{\perp}) \propto (1 - \cos K_{\perp}d)$ for a geometric terrace size distribution.^{27,40}

Our model shows a mixing of the properties of two-level and infinite-level surfaces. On one hand, we still observe a central component, although its intensity is very strong only close to the in-phase conditions if the rms height is large. On the other hand, Eq. (21) shows that the half-width of the shoulder has a cosine-like behavior close to the out-of-phase condition for $\alpha = 0.5$ (exponential correlation implying a geometric terrace size distribution) where the denominator can be neglected due to $w \gg d$. Here, on first sight, the infinite roughness $w = \infty$ seems to imply an infinite half-width. This is not the case since the infinite roughness causes also an infinite correlation length ξ so that the step density $\rho = 2w^2/\xi$ is finite.

Similar considerations are valid for oscillating correlation functions of infinite rough surfaces, which are caused by

sharp terrace size distributions. For instance, for a modified geometric terrace size distribution (cutting off small terrace sizes) it has been reported that the spots split into satellites close to the out-of-phase condition while the splitting vanishes close to the in-phase condition.²⁴ This effect is in agreement with our model as Eq. (30) demonstrates.

The roughness exponent α can be obtained from analyzing the phase dependence of the half-width of either the single shoulder for nonoscillating correlations or of the satellites for oscillating correlations. We would like to mention that the roughness $\alpha=0.5$ is implied by the models with noncorrelating next neighbor sizes. The interpretation that the half-width of the (Lorentzian) shoulder at the out-of-phase condition is proportional to the step density ρ is based upon these models. Therefore, it is an assumption that this interpretation holds still for larger roughness exponents used also by other authors.^{32,33} They have also shown that the step density ρ is constant for self-affine surfaces.

Recently, Amar and Family have studied both the autocovariance $w^2g(r)$ (called structure factor in their study) and the diffraction profiles at the out-of-phase condition in a MC simulation.⁴¹ Depending on the deposition condition, they observed self-affine surfaces (obeying scaling laws) and non-self-affine surfaces with peaks in the correlation functions (attributed to average mound sizes) and in the diffraction spots. They reported that also for the unstable growth the half-width of the out-of-phase satellites depends on the growth rate. Applying Eq. (22), this effect may be explained by different roughness exponents.

The roughness exponent is not involved in the phase dependence of the satellite position for oscillating correlations (non-self-affine surfaces). The oscillating height-height correlation implies the formation of pyramids and mounds on the surface.^{9,10} The average size of the pyramids $\langle\Lambda\rangle$ is attributed to the first minimum of the autocorrelation $g(r)$. Equivalently, we can identify the characteristic wave vector by $q_0=2\pi/\langle\Lambda\rangle$. Since the scaling law $\langle\Lambda\rangle\propto\Theta^n$ is proposed (similar to the correlation length for self-affine surfaces $\Theta^{1/z}$) we obtain the power law $k_0^{\text{out}}\propto\Theta^{\beta-n}$ for the satellite position at the out-of-phase condition. Following Eq. (15) and Eq. (31), the satellite position is determined by the step density for sharp terrace size distributions. Therefore, here we find a constant step density for $\beta=n$ as proposed by Siegert *et al.*⁸

Combining this with the relation for the out-of-phase satellite positions Eq. (30) and Eq. (15) (for sharp terrace size distributions), we obtain $d/\langle\Gamma\rangle=4(w/\langle\Lambda\rangle)$. This implies that the slope of the pyramid sides $m=w/\langle\Lambda\rangle$ and the local slope m_{local} defined by $m_{\text{local}}=d/\langle\Gamma\rangle=k_0^{\text{out}}d/\pi$ are proportional. This is expected for a surface with regular pyramids where the steps are either strictly upward or downward as Fig. 1 suggests. On the other hand, this simple relation is questionable for ‘‘real’’ surfaces with broader distributions of both pyramid and terrace sizes (cf. Fig. 15).

The key to this problem is that the satellite positions at the out-of-phase condition shift closer to the center of the Brillouin zone for broader distributions as Eq. (15) shows. Therefore π/k_0^{out} overestimates the average terrace size. We would like to mention that equivalent considerations as for the satellite position evaluation from the parameters of the terrace size distributions can be applied also for the height-height correlation of a surface with pyramids: the character-

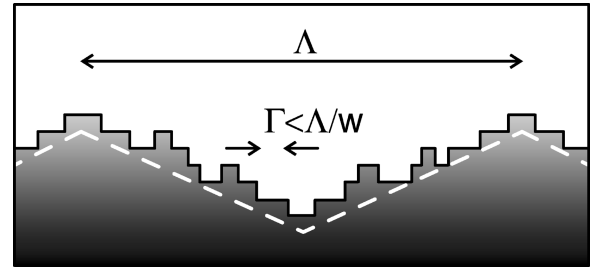


FIG. 15. Schematic drawing of pyramids with rough facets. The dashed white line shows the slope of the pyramid. Atomic steps form additional terraces so that the average terrace size Γ is less than the expected value Λ/w for regular facets with pure upward or downward staircases.

istic wave vector is smaller than $2\pi/\langle\Lambda\rangle$ if the pyramid size distribution is broad.⁴²

We have applied our model to analyze diffraction data obtained from the low temperature growth of homoepitaxial Ag films deposited on Ag(111) substrates. This proves that many roughness parameters can be obtained from the spot profile analysis. On one hand, it is well known that one obtains the rms height from the intensity of the central component. Using this as an input into Eq. (22) and Eq. (30), also the characteristic parameters of the height-height correlation can be evaluated. The splitting of the diffuse scattering into satellites shows that the film is grown under unstable growth conditions and pyramids are formed. The phase dependence of the satellite half-width reveals the roughness parameter $\alpha=0.5$, which we also obtain for the homoepitaxial growth on other fcc substrates.⁴³ This is different compared to MC simulation results proposing that the roughness exponent is slightly smaller than one for homoepitaxial growth on fcc(100) surfaces.^{9,10} Furthermore, in these and other studies¹⁸ a coarsening of the average pyramid size is reported for fcc(100) epitaxy. On the other hand, our analysis yields an almost constant characteristic wave vector for Ag/Ag(111) revealing a constant average size of the pyramids. This has also been reported by Ammer *et al.*³⁸

In conclusion, we derived a phenomenological model for the diffraction spot profile analysis of rough surfaces including oscillating correlations in the intermediate roughness range $d\ll w\ll\infty$. The diffraction spots split into a central component and a diffuse shoulder. Assuming a preserved vertical shape of the pair correlation, our analysis shows that not only the intensity of both, but also the parameters characterizing the diffuse shoulder (satellite position and half-width) depend on the scattering condition. This is confirmed by experiments. While one observes a single broad shoulder for self-affine surfaces formed under stable growth conditions, the diffuse scattering shows satellites or ringlike profiles for unstable growth conditions. From the phase dependence of the satellite half-width it is possible to obtain the roughness parameter α governing the height-height correlation for small lateral distances. The lateral roughness is described by different length scales, the average pyramid distance (long wavelength), and the average step-step distance (short wavelength). The diffraction experiment is sensitive to these different length scales at different scattering conditions. While the pyramid-pyramid distance can be obtained in principle from diffraction experiments per-

formed close to the in-phase condition, the experiment is sensitive to the step-step distances at the out-of-phase condition. Our analysis shows that both scales are mediated by the vertical roughness w and the lateral roughness exponent α . Since it is difficult to analyze spot profiles close to the in-phase condition easily (because of the weak diffuse intensity), these scaling laws provide a simple way to extract the long wavelength roughness from the out-of-phase profiles. We applied our model to the analysis of rough Ag films

grown on Ag(111) at low temperature where it grows in the statistical growth mode (vertical roughness $w \propto \Theta^{1/2}$). The appearance of satellites points to unstable growth conditions forming pyramids. We determined the roughness exponent $\alpha=0.5$ for these surfaces. Combining this with the power laws observed for the lateral roughness ($\kappa_{\text{out}} \propto k_0^{\text{out}} \propto \Theta^{2/3}$), we concluded an increasing correlation length ($\xi \propto \Theta^{1/3}$) and characteristic wave vector ($q_0 \propto \Theta^{1/6}$) pointing to an almost constant average pyramid size.

-
- ¹E. Bauer, *Z. Kristallogr.* **110**, 372 (1958).
²J. A. Venables, G. D. T. Stiller, and M. Hanbücken, *Rep. Prog. Phys.* **47**, 399 (1984).
³M. Henzler, *Prog. Surf. Sci.* **42**, 297 (1993).
⁴M. Henzler, T. Schmidt, and E. Z. Luo, in *Proceedings of the IV International Conference on the Structure of Surfaces*, edited by Xide Xie, S. Y. Tong, and M. A. Van Hove (World Scientific, Singapore, 1994), p. 619.
⁵M. Henzler, *Surf. Sci.* **357/358**, 809 (1996).
⁶H. N. Yang, G. C. Wang, and T. M. Lu, *Diffraction from Rough Surfaces and Dynamic Growth Fronts* (World Scientific, Singapore, 1993).
⁷J. Villain, *J. Phys. I* **1**, 19 (1991).
⁸M. Siegert and M. Plischke, *Phys. Rev. Lett.* **73**, 1517 (1994).
⁹P. Šmilauer and D. D. Vvedensky, *Phys. Rev. B* **52**, 14 263 (1995).
¹⁰M. Siegert and M. Plischke, *Phys. Rev. B* **53**, 307 (1996).
¹¹M. C. Bartelt and J. W. Evans, *Phys. Rev. Lett.* **75**, 4250 (1995).
¹²J. W. Evans and M. C. Bartelt, *Langmuir* **12**, 217 (1996).
¹³J. E. Van Nostrand, S. Jay Chey, M. A. Hasan, D. G. Cahill, and J. E. Greene, *Phys. Rev. Lett.* **74**, 1127 (1995).
¹⁴J. E. Van Nostrand, S. Jay Chey, M. A. Hasan, D. G. Cahill, and J. E. Greene, *Phys. Rev. B* **53**, 7876 (1996).
¹⁵H. J. Ernst, F. Fabre, R. Folkerts, and J. Lapujoulade, *Phys. Rev. Lett.* **72**, 112 (1994).
¹⁶Y. L. He, H. N. Yang, T. M. Lu, and G. C. Wang, *Phys. Rev. Lett.* **69**, 3770 (1992).
¹⁷J. A. Stroschio, D. T. Pierce, and R. A. Dragoset, *Phys. Rev. Lett.* **70**, 3615 (1993).
¹⁸J. A. Stroschio, D. T. Pierce, M. D. Stiles, A. Zangwill, and L. M. Sander, *Phys. Rev. Lett.* **75**, 4246 (1995).
¹⁹J. Wollschläger, J. Falta, and M. Henzler, *Appl. Phys. A: Solids Surf.* **50**, 57 (1990).
²⁰M. Henzler, *Surf. Sci.* **298**, 369 (1993).
²¹M. Henzler, in *Dynamical Phenomena at Surfaces, Interfaces, and Superlattices*, Springer Series in Surface Science Vol. 3, edited by F. Nizzoli, K. H. Rieder, and R. F. Willis (Springer, Berlin, 1985), p. 14.
²²M. G. Lagally, D. E. Savage, and M. C. Tringides, in *Reflection High-Energy Electron Diffraction and Reflection Imaging of Surfaces*, edited by P. K. Larsen and P. J. Dobson (Plenum, New York, 1988), p. 139.
²³M. Henzler, in *The Structure of Surfaces II*, Springer Series in Surface Science Vol. 11, edited by F. van der Veen and M. A. Van Hove (Springer, Berlin, 1988), p. 431.
²⁴J. M. Pimbley and T. M. Lu, *Surf. Sci.* **159**, 169 (1985).
²⁵J. Wollschläger, *Surf. Sci.* **383**, 103 (1997).
²⁶C. S. Lent and P. I. Cohen, *Surf. Sci.* **139**, 121 (1984).
²⁷P. R. Pukite, C. S. Lent, and P. I. Cohen, *Surf. Sci.* **167**, 39 (1985).
²⁸J. M. Pimbley and T. M. Lu, *J. Vac. Sci. Technol. A* **2**, 457 (1984).
²⁹J. M. Pimbley and T. M. Lu, *J. Appl. Phys.* **57**, 1121 (1984).
³⁰J. M. Pimbley and T. M. Lu, *J. Appl. Phys.* **55**, 182 (1984).
³¹S. K. Sinha, E. B. Sirota, S. Garoff, and H. B. Stanley, *Phys. Rev. B* **38**, 2297 (1988).
³²H. N. Yang, T. M. Lu, and G. C. Wang, *Phys. Rev. Lett.* **68**, 2612 (1992).
³³H. N. Yang, T. M. Lu, and G. C. Wang, *Phys. Rev. B* **47**, 3911 (1993).
³⁴R. Altsinger, H. Busch, M. Horn, and M. Henzler, *Surf. Sci.* **200**, 235 (1988).
³⁵J. Villain, D. R. Grempel, and J. Lapujoulade, *J. Phys. F* **15**, 809 (1985).
³⁶G. Meyer, J. Wollschläger, and M. Henzler, *Surf. Sci.* **231**, 64 (1990).
³⁷S. Fölsch, B. Ch. Choi, and K. H. Rieder, *Phys. Rev. B* **54**, 10 855 (1996).
³⁸Ch. Ammer, T. Schaefer, Ch. Teichert, K. Meinel, and M. Klaua, *Surf. Sci.* **307-309**, 570 (1994).
³⁹E. Z. Luo, J. Wollschläger, F. Wegner, and M. Henzler, *Appl. Phys. A: Mater. Sci. Process.* **60**, 60 (1995).
⁴⁰T. M. Lu and M. G. Lagally, *Surf. Sci.* **120**, 47 (1982).
⁴¹J. G. Amar and F. Family, *Surf. Sci.* **365**, 177 (1996).
⁴²J. Wollschläger and S. Fölsch (unpublished).
⁴³J. Wollschläger, T. Schmidt, and M. Henzler (unpublished).